Prepared for submission to JCAP

The effect of Limber and flat-sky approximations on galaxy weak lensing

Pablo Lemos,[a] **Anthony Challinor,**[a,b] **and George Efstathiou.**[a]

[a]Institute of Astronomy and Kavli Institute for Cosmology Cambridge, Madingley Road, Cambridge CB3 OHA, UK
[b]DAMTP, Centre for Mathematical Sciences, Wilberforce Road, Cambridge CB3 0WA, UK

E-mail: pl411@cam.ac.uk, a.d.challinor@ast.cam.ac.uk, gpe@ast.cam.ac.uk

Abstract. We review the effect of the commonly-used Limber and flat-sky approximations on the calculation of shear power spectra and correlation functions for galaxy weak lensing. These approximations are accurate at small scales, but it has been claimed recently that their impact on low multipoles could lead to an increase in the amplitude of the mass fluctuations inferred from surveys such as CFHTLenS, reducing the tension between galaxy weak lensing and the amplitude determined by Planck from observations of the cosmic microwave background. Here, we explore the impact of these approximations on cosmological parameters derived from weak lensing surveys, using the CFHTLenS data as a test case. We conclude that the use of small-angle approximations for cosmological parameter estimation is negligible for current data, and does not contribute to the tension between current weak lensing surveys and Planck.[1]

[1]As this paper was nearing completion, analyses were presented by Kilbinger et al. [1] and in the revised version of Kitching et al. [2] with similar conclusions to ours.

Contents

1 Introduction

The amplitude and shape of the mass fluctuation spectrum is of fundamental importance to cosmology. The mass fluctuation spectrum can be used to test the physics of the early Universe, its contents, and the nature of gravity. In addition, it determines the timescales and evolutionary paths for the formation of non-linear objects such as galaxies and galaxy clusters that we see in the Universe today.

Observations of the cosmic microwave background (CMB) [3, 4] have led to precision measurements of the shape of the fluctuation spectrum and via gravitational lensing of the CMB can constrain its amplitude down to redshifts $z \sim 2$. Determining the amplitude at lower redshifts is, however, challenging. Weak gravitational lensing of galaxies is a particularly promising technique. Several weak lensing analyses [5–9] have reported constraints on the amplitude of the fluctuation spectrum as measured by the parameter σ_8.[1] The results from two surveys, CFHTLenS [7] and KiDS [8], are discrepant with the Planck constraints on the parameter combination $\sigma_8\Omega_m^{0.5}$, where Ω_m is the present-day matter density parameter, at about the $2.5\,\sigma$ level, assuming the standard six-parameter ΛCDM cosmology (which we will refer to as the base-ΛCDM model). The possibility of new physics beyond base-ΛCDM [10] merits close scrutiny of both the weak lensing and CMB data.

Recently, Ref. [2] investigated the Limber approximation [11] and a number of other small-angle approximations used to relate weak lensing observables to the three-dimensional matter power spectrum. The first version of that paper concluded that such approximations could contribute significantly to the tension between the CMB measurements and weak lensing data. This conclusion, if correct, would have important implications for cosmology and motivated the analysis presented in this paper.

The paper is structured as follows. In Sec. 2 we derive the full two-point statistics for weak galaxy lensing in different tomographic redshift bins in full generality, i.e., without using flat-sky or Limber-like approximations (extending the work of Refs [12, 13]). We then compare the exact formulae to small-angle approximations. Section 3 applies these formulae

[1] Here, σ_8 is the rms amplitude of the mass fluctuations in spheres of radius $8h^{-1}\,\mathrm{Mpc}$, where h is the Hubble constant in units of $100\,\mathrm{km\,s^{-1}\,Mpc^{-1}}$.

to the latest tomographic weak lensing data from CFHTLenS[2] [7] and assesses the impact of these approximations on cosmological parameters and on the tension with the base-ΛCDM constraints from Planck. Our conclusions are presented in Sec. 4. Appendix A provides more detail on some of the results used in the main text.

2 Two-point statistics

Our aim in this section is to present exact expressions for two-point weak lensing statistics and then to apply small-angle approximations. Further details of the calculations that underlie these results are given in the appendix. Throughout, we assume a spatially-flat universe.

We start from the definition of the lensing potential $\phi(\hat{\boldsymbol{n}})$ as a function of the gravitational potential $\Phi(\boldsymbol{x}, \chi)$ at (comoving) position $\boldsymbol{x}$ and lookback time χ, integrated along the line-of-sight $\hat{\boldsymbol{n}}$ and weighted by a redshift distribution $n(\chi)$ of lensing sources:

$$\phi(\hat{\boldsymbol{n}}) = \frac{2}{c^2} \int \frac{\mathrm{d}\chi}{\chi} q(\chi) \Phi(\chi\hat{\boldsymbol{n}}, \chi), \tag{2.1}$$

where χ is the comoving radial distance. In this equation $n(\chi)$ is normalized so that $\int n(\chi)\, d\chi = 1$ and $q(\chi)$ is the lensing efficiency:

$$q(\chi) = \int_{\chi}^{\chi_H} \mathrm{d}\chi' \, \frac{\chi' - \chi}{\chi'} n(\chi'), \tag{2.2}$$

where χ_H is the distance to the particle horizon.

We are interested in the two-point statistic

$$\left\langle \phi(\hat{\boldsymbol{n}}) \phi(\hat{\boldsymbol{n}}') \right\rangle = \left(\frac{2}{c^2} \right)^2 \int \frac{\mathrm{d}\chi}{\chi} q(\chi) \int \frac{\mathrm{d}\chi'}{\chi'} q(\chi') \left\langle \Phi(\chi\hat{\boldsymbol{n}}, \chi) \Phi(\chi'\hat{\boldsymbol{n}}', \chi') \right\rangle . \tag{2.3}$$

Expanding the two-dimensional lensing potential ϕ in spherical harmonics, and the gravitational potential in Fourier modes, and using Poisson's equation, we can relate the lensing angular power spectrum $C_\ell^{\phi\phi}$,

$$\langle \phi_{\ell m} \phi_{\ell' m'} \rangle = C_\ell^{\phi\phi} \delta_{\ell\ell'} \delta_{mm'}, \tag{2.4}$$

to the unequal-time dimensional matter power spectrum $P_\delta(k; \chi, \chi')$. If we further approximate the unequal-time power spectrum as separable (which is exact in linear theory; see [14] for the impact of non-linear evolution), i.e.,

$$P_\delta(k; \chi, \chi') \approx \left[P_\delta(k; \chi) P_\delta(k; \chi') \right]^{1/2}, \tag{2.5}$$

for two tomographic redshift bins (r, s) with redshift distributions $n^r(\chi)$ and $n^s(\chi)$ we find

$$C_\ell^{\phi\phi}(r, s) = \frac{8}{\pi} \left(\frac{3\Omega_m H_0^2}{2c^2} \right)^2 \int \frac{\mathrm{d}k}{k^2} \, I_\ell^r(k) I_\ell^s(k), \tag{2.6a}$$

where

$$I_\ell^r(k) = \int \frac{\mathrm{d}\chi}{\chi} \left[1 + z(\chi) \right] q^r(\chi) j_\ell(k\chi) \left[P_\delta(k; \chi) \right]^{1/2} . \tag{2.6b}$$

[2]The data used in this paper is publicly available at https://github.com/sjoudaki/cfhtlens_revisited.

The main observable in weak galaxy lensing surveys is the shear, which can be described by the spin-2 field $\gamma = \eth^2\phi/2$, where $\eth$ is the spin-raising operator [15]. The expansions of the shear, and its complex conjugate, in spin ± 2 spherical harmonics are

$$\gamma(\hat{\boldsymbol{n}}) = \sum_{\ell m}(\epsilon_{\ell m} + i\beta_{\ell m})\,{}_2Y_{\ell m}(\hat{\boldsymbol{n}}), \tag{2.7}$$

$$\gamma^*(\hat{\boldsymbol{n}}) = \sum_{\ell m}(\epsilon_{\ell m} - i\beta_{\ell m})\,{}_{-2}Y_{\ell m}(\hat{\boldsymbol{n}}), \tag{2.8}$$

where $\epsilon_{\ell m}$ are the multipoles of the E-mode of the shear and $\beta_{\ell m}$ for the B-modes. For lensing in the Born approximation, as considered here, the gravitational shear has only E-modes with $\epsilon_{\ell m} = \sqrt{(\ell+2)!/(\ell-2)!}\phi_{\ell m}/2$. The angular power spectrum of the lensing potential, Eq. (2.6a), can easily be related to the E-mode power spectrum of the shear field by

$$C_\ell^{\epsilon\epsilon} = \frac{1}{4}\frac{(\ell+2)!}{(\ell-2)!}C_\ell^{\phi\phi}. \tag{2.9}$$

The shear γ is defined relative to the θ and ϕ directions. The two-point functions of the shear in real space are simplest when the shear at the two points, $\hat{\boldsymbol{n}}_1$ and $\hat{\boldsymbol{n}}_2$, are rotated onto bases generated by the great circle through the two points (and the orthogonal directions). If we denote the rotated shear by an overbar, e.g., $\bar{\gamma}(\hat{\boldsymbol{n}}_1)$, the shear correlation functions for tomographic bins r and s are defined as

$$\xi_+(\theta; r, s) = \langle\bar{\gamma}_r^*(\hat{\boldsymbol{n}}_1)\bar{\gamma}_s(\hat{\boldsymbol{n}}_2)\rangle\,, \qquad \xi_-(\theta; r, s) = \langle\bar{\gamma}_r(\hat{\boldsymbol{n}}_1)\bar{\gamma}_s(\hat{\boldsymbol{n}}_2)\rangle, \tag{2.10}$$

where θ is the angle between $\hat{\boldsymbol{n}}_1$ and $\hat{\boldsymbol{n}}_2$. The $\xi_\pm$ can be expressed in terms of the shear power spectrum as (see appendix A.2)[3]

$$\xi_+(\theta; r, s) = \sum_\ell \frac{2\ell+1}{4\pi}C_\ell^{\epsilon\epsilon}(r, s)d^l_{2\,2}(\theta), \tag{2.11a}$$

$$\xi_-(\theta; r, s) = \sum_\ell \frac{2\ell+1}{4\pi}C_\ell^{\epsilon\epsilon}(r, s)d^\ell_{2\,-2}(\theta), \tag{2.11b}$$

where d^ℓ_{mn} are the reduced Wigner D-matrices. The equations above are all exact and make no use of the Limber or flat-sky approximations.

2.1 Limber approximation

The exact expressions for the power spectra, Eqs. (2.6a) and (2.6b) are time consuming to evaluate accurately at high multipoles due to the rapid oscillations of the spherical Bessel functions. Many analyses adopt the Limber approximation instead, which is accurate at large ℓ and much easier to compute. In the Limber approximation, we effectively replace the spherical Bessel function in Eq. (2.6b) with a delta-function,

$$j_\ell(k\chi) \to \sqrt{\frac{\pi}{2\nu}}\delta_D(\nu - k\chi), \tag{2.12}$$

[3]Equation (48) of Ref. [1] incorrectly has the $d^\ell_{2\,2}$ replaced by Legendre polynomials in the expression for the spherical $\xi_+(\theta; r, s)$. This introduces errors that increase steadily with θ. However, for our application to CFHTLenS (Sec. 3) the error is below 2 % on the relevant scales ($\theta < 100$ arcmin) and so does not affect the conclusions of Ref. [1].

where $\nu = \ell + 1/2$. The wavenumber k is then related to radial distance χ via the relation $k\chi = \nu$. This approximation is accurate if the rest of the integrand in Eq. (2.6b) is slowly varying compared to the spherical Bessel function, which is generally the case at large ℓ (see [12] for a careful discussion). Making this approximation in Eq. (2.6b), and using Eqs. (2.6a) and (2.9), we recover the familiar Limber formula for the shear power spectrum

$$C_\ell^{\epsilon\epsilon}(r,s) = \frac{(\ell+2)!}{\nu^4(\ell-2)!}\left(\frac{3\Omega_m H_0^2}{2c^2}\Omega_m\right)^2 \int \mathrm{d}\chi\,[1+z(\chi)]^2\, q^r(\chi) q^s(\chi) P_\delta(\nu/\chi;\chi). \tag{2.13}$$

2.2 Flat-sky approximations

Mathematically, the flat-sky approximations consist of replacing the expansion in spherical harmonics by an expansion in Fourier modes. The relation between shear and lensing power spectra, Eq. (2.9), is then

$$C_\ell^{\epsilon\epsilon} \approx \frac{\ell^4}{4} C_\ell^{\phi\phi}. \tag{2.14}$$

The reduced D-matrices for high multipoles can be approximated by Bessel functions [16]:

$$d^\ell_{2\ +2}(\theta) \approx J_0(\ell\theta) \qquad d^\ell_{2\ -2}(\theta) \approx J_4(\ell\theta), \tag{2.15}$$

and together with the Limber-approximated expression (2.13), we obtain the usual expression for the shear power spectrum [17]

$$C_\ell^{\epsilon\epsilon}(r,s) = \left(\frac{3\Omega_m H_0^2}{2c^2}\right)^2 \int \mathrm{d}\chi\ [1+z(\chi)]^2\, q^r(\chi) q^s(\chi) P_\delta(\nu/\chi;\chi), \tag{2.16a}$$

and the correlation functions

$$\xi_+(\theta,r,s) = \frac{1}{2\pi}\int \mathrm{d}\ell\ell J_0(\ell\theta) C_\ell^{\epsilon\epsilon}(r,s), \tag{2.16b}$$

$$\xi_-(\theta,r,s) = \frac{1}{2\pi}\int \mathrm{d}\ell\ell J_4(\ell\theta) C_\ell^{\epsilon\epsilon}(r,s). \tag{2.16c}$$

Note that we have replaced ν by ℓ in the prefactor of the Limber-approximated power spectrum, Eq. (2.13), and also in the expressions (2.11a) and (2.11b) for the correlation functions $[(2\ell+1)/(4\pi) \to \ell/(2\pi)]$. We have, however, retained ν in the argument of the matter power spectrum.

In this paper, we compare exact results with two flat-sky approximations: (i) Equations (2.16a–2.16c) with $\nu = (\ell + 1/2)$ in the argument of the matter power spectrum, which is the approximation used in the tomographic analysis of CFHTlenS and KiDS weak lensing data[4] (we call this 'flat-sky no prefactor'); and (ii) Equations (2.13), and (2.16b–2.16c) with $\nu = (\ell + 1/2)$ in both the prefactor and the matter power spectrum (which we call 'flat-sky with prefactor'). These two approximations differ from each other only in the prefactor of the shear power spectrum. The spectrum with the prefactor is smaller by a factor of approximately $1 - 5/(2\ell^2)$. We shall compare each of these approximations to the exact expressions (2.6a–2.6b) and (2.11a–2.11b).

[4]Note that Eq. (4) in [8] uses $\nu = \ell$ in the argument of the matter power spectrum; however, the public KiDS likelihood code uses $\nu = \ell + 1/2$.

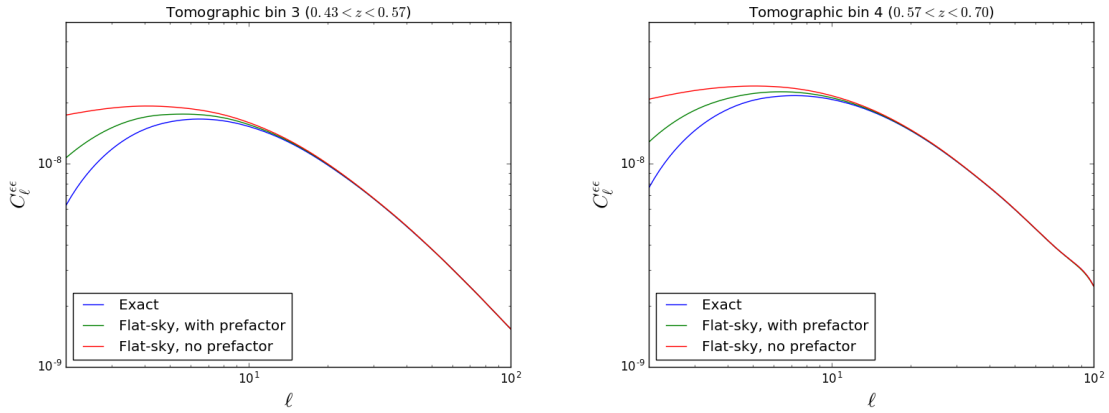

Figure 1. Shear power spectra for the third (left) and fourth (right) tomographic redshift bins of the revised CFHTLenS data set assuming the best-fit parameters of [7], illustrating the effects of the small-angle approximations discussed in the text. The red lines use the same approximations as in the tomographic analyses of the CFHTLenS and KiDS weak lensing data, while the blue lines are from the exact calculation.

3 Application to CFHTLenS data

In this section we investigate the impact of the small-angle approximations on current weak lensing parameter constraints using the CFHTLenS survey as an example. CFHTLenS is based on imaging data from the Canada-France-Hawaii telescope in five photometric bands. In the reanalysis of [7], the data is divided into seven tomographic redshift bins with photometric redshifts spanning the range $0.15 < z < 1.30$. We use the calibrated redshift distributions to compute the exact shear power spectrum, as well as the 'flat-sky no prefactor' and the 'flat-sky with prefactor' spectra, using the formulae presented in the previous section assuming the best-fit parameters of [7]. Figure 1 shows the resulting shear power spectra for the third and fourth tomographic redshift bins. This shows that the small-angle approximations have negligible impact except at multipoles $\ell \lesssim 10$. However, the CFHTLenS analyses are insensitive to these multipoles.

We can see explicitly that the small-angle approximations have negligible impact on the CFHTLens analysis by looking at the shear correlation functions ξ_+ and ξ_-. Figure 2 shows the predictions for ξ_+ and ξ_- for the various approximations assuming the best-fit parameters of [7] for tomographic redshift bin 3, together with the data points and $1\,\sigma$ errors from [7]. Compared to the large errors on the CFHTLenS data points, the effects of adopting small-angle approximations are negligible over the angular scales probed by the data.

As a final test, we perform parameter estimation (with CosmoMC [18, 19]) sampling the CFHTLenS likelihood as in [7] comparing the 'flat-sky prefactor' with the 'flat-sky no prefactor' approximations.[5] As expected from Fig. 1, the impact of these approximations on cosmological parameters such as σ_8 and Ω_m is undetectable within the convergence errors of the parameter chains (and therefore well below the $1\,\sigma$ errors on cosmological parameters).

[5]We have not tested the exact calculation since it is too slow to be used in CosmoMC. However, the differences between the exact correlation functions and those with the 'flat-sky no prefactor' approximation are about twice as large as the differences between the two flat-sky approximations, so our analysis should still be representative of the actual errors introduced by the small-angle approximations.

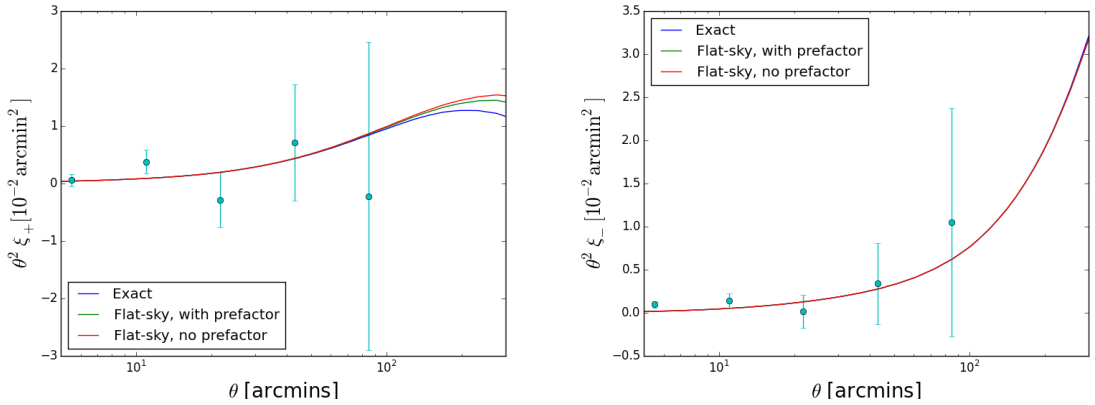

Figure 2. Shear correlation functions ξ_+ (left) and ξ_- (right) for the third tomographic redshift bin of CFHTLenS. The points show the CFHTLenS measurements together with $1\,\sigma$ errors. The model curves show the effects of the small-angle approximations described in the text, assuming the best-fit parameters of [7].

4 Conclusions

The analysis presented here shows that the small-angle Limber and flat-sky approximations that are typically used in the analysis of galaxy weak lensing have no significant impact on cosmological parameters derived from current data. Kilbinger et al. [1] have reached similar conclusions recently, as does the revised version of [2]. Three independent analyses are therefore in agreement that small-angle approximations have no bearing on the discrepancy between the amplitude of the mass fluctuation spectrum inferred from the CFHTLenS or KiDS galaxy weak lensing data and that measured from the CMB assuming the base-ΛCDM cosmology.

Acknowledgments

Pablo Lemos acknowledges support from an Isaac Newton Studentship at the University of Cambridge and from the Science and Technologies Facilities Council (STFC). We thank Patricia Larsen for helpful discussions.

A Galaxy weak lensing two-point statistics

In this appendix we summarise results for the two-point statistics of the weak lensing observables, namely convergence and shear, on the spherical sky and also in the flat-sky limit. These results are valid for both weak lensing of galaxies and of the CMB. As in the main text, we assume a flat universe throughout.

All weak lensing quantities can be defined as a function of the lensing potential $\phi(\hat{\boldsymbol{n}}, \chi)$ for sources at comoving distance χ:

$$\phi(\hat{\boldsymbol{n}}, \chi) = \frac{2}{c^2} \int_0^\chi \mathrm{d}\chi' \, \frac{\chi - \chi'}{\chi \chi'} \Phi(\chi' \hat{\boldsymbol{n}}, \chi'), \tag{A.1}$$

where $\Phi(\boldsymbol{x}, \chi)$ is the gravitational potential at comoving position $\boldsymbol{x}$ and conformal lookback time χ.

If we average observables over sources with a redshift distribution $n(\chi)$, normalised such that $\int n(\chi)\,\mathrm{d}\chi = 1$, the relevant 2D lensing potential is given by

$$\phi(\hat{\boldsymbol{n}}) = \int \mathrm{d}\chi\, n(\chi)\phi(\hat{\boldsymbol{n}},\chi) = \frac{2}{c^2}\int \frac{\mathrm{d}\chi'}{\chi'} q(\chi')\Phi(\chi'\hat{\boldsymbol{n}},\chi'), \tag{A.2}$$

where $q(\chi)$ is the lensing efficiency defined in Eq. (2.2). In the case of CMB lensing, the source distribution can be approximated by a delta-function at the surface of last scattering: $n(\chi) = \delta_D(\chi - \chi_*)$. The lensing potential is a scalar field and can be expanded in spherical harmonics as

$$\phi(\hat{\boldsymbol{n}}) = \sum_{\ell,m} \phi_{\ell m} Y_\ell^m(\hat{\boldsymbol{n}}). \tag{A.3}$$

The basic observables in weak lensing are the convergence κ and the components γ_1 and γ_2 of the shear, defined in terms of the second derivatives of the lensing potential as

$$\nabla_i\nabla_j\phi = \kappa g_{ij} + \frac{1}{2}(\gamma_1 + i\gamma_2)(\boldsymbol{m}_- \otimes \boldsymbol{m}_-)_{ij} + \frac{1}{2}(\gamma_1 - i\gamma_2)(\boldsymbol{m}_+ \otimes \boldsymbol{m}_+)_{ij}, \tag{A.4}$$

where g_{ij} is the metric on the sphere and the null vectors $\boldsymbol{m}_\pm = \hat{\boldsymbol{\theta}} \pm i\hat{\boldsymbol{\phi}}$. Here, $\hat{\boldsymbol{\theta}}$ and $\hat{\boldsymbol{\phi}}$ are unit vectors along the θ and ϕ coordinate directions of a spherical-polar coordinate system. The convergence $\kappa = \nabla^2\phi/2$ describes isotropic magnification/dilation and is a scalar field. The shear describes area-preserving distortions; the complex shear $\gamma = \gamma_1 + i\gamma_2$ is a spin-2 field related to the lensing potential via

$$\gamma = \frac{1}{2}(\boldsymbol{m}_+ \otimes \boldsymbol{m}_+)_{ij}\nabla^i\nabla^j\phi = \frac{1}{2}\eth^2\phi, \tag{A.5}$$

where $\eth$ is the spin-raising operator [15]. The spherical-harmonic expansions of the convergence and shear follow from Eq. (A.3):

$$\kappa(\hat{\boldsymbol{n}}) = -\frac{1}{2}\sum_{\ell,m} \ell(\ell+1)\phi_{\ell m} Y_\ell^m(\hat{\boldsymbol{n}}), \tag{A.6a}$$

$$\gamma_1(\hat{\boldsymbol{n}}) \pm i\gamma_2(\hat{\boldsymbol{n}}) = \frac{1}{2}\sum_{\ell,m} \sqrt{\frac{(\ell+2)!}{(\ell-2)!}}\phi_{\ell m}\, {}_{\pm2}Y_\ell^m(\hat{\boldsymbol{n}}). \tag{A.6b}$$

Generally, a spin 2 field can be expanded in E- and B-modes, for example,

$$(\gamma_i \pm i\gamma_2)(\hat{\boldsymbol{n}}) = \sum_{\ell,m} (\epsilon_{\ell m} \pm i\beta_{\ell m})\, {}_{\pm2}Y_\ell^m(\hat{\boldsymbol{n}}), \tag{A.7}$$

where $\epsilon_{\ell m}$ are the E-mode multipoles and $\beta_{\ell m}$ are the B-mode multipoles. These transform oppositely under parity: $\epsilon_{\ell m} \to (-1)^\ell \epsilon_{\ell m}$ and $\beta_{\ell m} \to (-1)^{\ell+1}\beta_{\ell m}$. However, we see from Eq. (A.6b) that the gravitational shear has no B-modes (in the Born approximation that we are assuming here), while $\epsilon_{\ell m} = \sqrt{(\ell+2)!/(\ell-2)!}\phi_{\ell m}/2$.

The angular power spectrum of the lensing potential is defined by

$$\langle \phi_{\ell m}\phi^*_{\ell' m'}\rangle = \delta_{\ell\ell'}\delta_{mm'}C_\ell^{\phi\phi}. \tag{A.8}$$

We can similarly define the convergence and shear power, which are related to $C_\ell^{\phi\phi}$ by

$$C_\ell^{\kappa\kappa} = \frac{\ell^2(\ell+1)^2}{4} C_\ell^{\phi\phi}, \tag{A.9a}$$

$$C_\ell^{\epsilon\epsilon} = \frac{1}{4}\frac{(\ell+2)!}{(\ell-2)!} C_\ell^{\phi\phi}. \tag{A.9b}$$

In the flat-sky approximation, we project onto the tangent plane at the centre of the observed field and denote positions in this plane with a 2D vector $\boldsymbol{\theta}$. Expansions in spherical harmonics are replaced by Fourier expansions, so that for the gravitational potential

$$\phi(\boldsymbol{\theta}) = \int \frac{\mathrm{d}^2\boldsymbol{l}}{(2\pi)^2}\, \phi(\boldsymbol{l}) e^{i\boldsymbol{l}\cdot\boldsymbol{\theta}}. \tag{A.10}$$

The expansions of the convergence and shear become

$$\kappa(\boldsymbol{\theta}) = -\frac{1}{2}\int \frac{\mathrm{d}^2\boldsymbol{l}}{(2\pi)^2}\, l^2\phi(\boldsymbol{l}) e^{i\boldsymbol{l}\cdot\boldsymbol{\theta}} \tag{A.11a}$$

$$(\gamma_1 \pm i\gamma_2)(\boldsymbol{\theta}) = -\frac{1}{2}\int \frac{\mathrm{d}^2\boldsymbol{l}}{(2\pi)^2}\, l^2\phi(\boldsymbol{l}) e^{\pm 2i(\psi_{\boldsymbol{l}} - \psi_{\boldsymbol{\theta}})} e^{i\boldsymbol{l}\cdot\boldsymbol{\theta}}, \tag{A.11b}$$

where $\psi_{\boldsymbol{l}}$ and $\psi_{\boldsymbol{\theta}}$ are the angles that $\boldsymbol{l}$ and $\boldsymbol{\theta}$, respectively, make with the x-axis. Note that the components of the shear are defined relative to a polar-coordinate basis in the plane; rotating to a global Cartesian basis removes the factors of $e^{\mp 2i\psi_{\boldsymbol{\theta}}}$.

In the flat-sky approximation, the power spectra are related simply by

$$C_\ell^{\kappa\kappa} = \frac{\ell^4}{4} C_\ell^{\phi\phi} = \frac{\ell^4}{4} C_\ell^{\epsilon\epsilon}. \tag{A.12}$$

A.1 Relation to the matter power spectrum

We can relate the lensing angular power spectra to the 3D matter power spectra as follows. We begin by expanding the gravitational potential in Eq. (A.2) in Fourier modes $\Phi(\boldsymbol{k}, \chi)$ and using the plane-wave expansion to find

$$\phi_{\ell m} = i^\ell \frac{8\pi}{c^2} \int \frac{\mathrm{d}^3\boldsymbol{k}}{(2\pi)^3} \left(\int \frac{\mathrm{d}\chi}{\chi}\, q(\chi) j_\ell(k\chi) \Phi(\boldsymbol{k}, \chi) \right) Y_\ell^{m*}(\hat{\boldsymbol{k}})\,. \tag{A.13}$$

The two-point correlator of the gravitational potential is

$$\langle \Phi(\boldsymbol{k}, \chi) \Phi^*(\boldsymbol{k}', \chi') \rangle = (2\pi)^3 P_\Phi(k; \chi, \chi') \delta_D^{(3)}(\boldsymbol{k} - \boldsymbol{k}'), \tag{A.14}$$

where $P_\Phi(k; \chi, \chi')$ is the unequal-time power spectrum of the gravitational potential. It follows from Eq. (A.13) that, for redshift distributions $q^r(\chi)$ and $q^s(\chi)$,

$$C_\ell^{\phi\phi}(r, s) = \left(\frac{8\pi}{c^2}\right)^2 \int \frac{k^2 \mathrm{d}k}{(2\pi)^3} \int \frac{\mathrm{d}\chi}{\chi} q^r(\chi) j_\ell(k\chi) \int \frac{\mathrm{d}\chi'}{\chi'} q^s(\chi') j_\ell(k\chi') P_\Phi(k; \chi, \chi'). \tag{A.15}$$

This simplifies if we adopt the approximation made in the main text,

$$P_\Phi(k; \chi, \chi') \approx \left[P_\Phi(k; \chi) P_\Phi(k; \chi') \right]^{1/2}, \tag{A.16}$$

to give

$$C_\ell^{\phi\phi}(r,s) = \frac{8}{\pi c^4}\int k^2 \mathrm{d}k\, \hat{I}_\ell^r(k)\hat{I}_\ell^s(k), \tag{A.17}$$

where

$$\hat{I}_\ell^r(k) = \int \frac{\mathrm{d}\chi}{\chi} q^r(\chi) j_\ell(k\chi)\left[P_\Phi(k,\chi)\right]^{1/2}. \tag{A.18}$$

Finally, we can relate the 3D power spectrum of the gravitational potential to the 3D matter power spectrum using Poisson's equation, i.e.,

$$P_\Phi(k;\chi) = \left(\frac{3}{2}\Omega_m H_0^2\left[1+z(\chi)\right]\right)^2 \frac{P_\delta(k;\chi)}{k^4}, \tag{A.19}$$

to obtain our final result

$$C_\ell^{\phi\phi}(r,s) = \frac{8}{\pi}\left(\frac{3\Omega_m H_0^2}{2c^2}\right)^2 \int \frac{\mathrm{d}k}{k^2}\, I_\ell^r(k) I_\ell^s(k), \tag{A.20a}$$

$$I_\ell^r(k) = \int \frac{\mathrm{d}\chi}{\chi}\left[1+z(\chi)\right] q^r(\chi) j_\ell(k\chi)\left[P_\delta(k,\chi)\right]^{1/2}. \tag{A.20b}$$

A.2 Spherical correlation functions

Expressions for the spherical correlation functions of the gravitational shear from the angular power spectrum can be obtained following the methods used for CMB polarization (also a spin-2 field) in Refs. [20, 21]. To maintain generality, we give results including B-modes although, as noted above, these are expected to vanish for the gravitational shear.

As discussed in the main text, the correlation functions of the shear for lines of sight $\hat{\boldsymbol{n}}_1$ and $\hat{\boldsymbol{n}}_2$ are simplest when the shear is expressed at each point in bases generated by the great circle through the two points. If α_1 is the angle require to rotate $\hat{\boldsymbol{\theta}}_1$ in a right-handed sense about $\hat{\boldsymbol{n}}_1$ onto the tangent to the great circle there, the rotated shear is $\bar{\gamma}(\hat{\boldsymbol{n}}_1) = e^{-2i\alpha_1}\gamma(\hat{\boldsymbol{n}}_1)$. For redshift distributions $q^r(\chi)$ and $q^s(\chi)$, the two-point correlation functions of the rotated shear are

$$\xi_+(\theta;r,s) = \langle \bar{\gamma}_r^*(\hat{\boldsymbol{n}}_1)\bar{\gamma}_s(\hat{\boldsymbol{n}}_2)\rangle = \sum_\ell \frac{2\ell+1}{4\pi}\left[C_\ell^{\epsilon\epsilon}(r,s) + C_\ell^{\beta\beta}(r,s)\right] d^l_{2\,2}(\theta), \tag{A.21a}$$

$$\xi_-(\theta;r,s) = \langle \bar{\gamma}_r(\hat{\boldsymbol{n}}_1)\bar{\gamma}_s(\hat{\boldsymbol{n}}_2)\rangle = \sum_\ell \frac{2\ell+1}{4\pi}\left[C_\ell^{\epsilon\epsilon}(r,s) - C_\ell^{\beta\beta}(r,s)\right] d^\ell_{2\,-2}(\theta), \tag{A.21b}$$

where d^ℓ_{mn} are the reduced Wigner D-matrices, and θ is the angle between $\hat{\boldsymbol{n}}_1$ and $\hat{\boldsymbol{n}}_2$. The correlation coefficients for the shear components follow from these expressions (noting that the right-hand sides are real-valued):

$$\langle \bar{\gamma}_{1,r}(\hat{\boldsymbol{n}}_1)\bar{\gamma}_{1,s}(\hat{\boldsymbol{n}}_2)\rangle = \frac{1}{2}\left[\xi_+(\theta;r,s) + \xi_-(\theta;r,s)\right], \tag{A.22a}$$

$$\langle \bar{\gamma}_{2,r}(\hat{\boldsymbol{n}}_1)\bar{\gamma}_{2,s}(\hat{\boldsymbol{n}}_2)\rangle = \frac{1}{2}\left[\xi_+(\theta;r,s) - \xi_-(\theta;r,s)\right]. \tag{A.22b}$$

Correlations between mixed components, e.g., $\langle \bar{\gamma}_{1,r}(\hat{\boldsymbol{n}}_1)\bar{\gamma}_{2,s}(\hat{\boldsymbol{n}}_2)\rangle$, vanish since we are assuming that parity invariance holds in the mean (so that $C_\ell^{\epsilon\beta}(r,s) = 0$).

References

[1] M. Kilbinger, C. Heymans, M. Asgari, S. Joudaki, P. Schneider, P. Simon et al., *Precision calculations of the cosmic shear power spectrum projection*, *ArXiv e-prints* (Feb., 2017) , [1702.05301].

[2] T. D. Kitching, J. Alsing, A. F. Heavens, R. Jimenez, J. D. McEwen and L. Verde, *The Limits of Cosmic Shear*, *ArXiv e-prints* (Nov., 2016) , [1611.04954].

[3] Planck Collaboration, P. A. R. Ade, N. Aghanim, C. Armitage-Caplan, M. Arnaud, M. Ashdown et al., *Planck 2013 results. XVI. Cosmological parameters*, *A&A* **571** (Nov., 2014) A16, [1303.5076].

[4] Planck Collaboration, P. A. R. Ade, N. Aghanim, M. Arnaud, M. Ashdown, J. Aumont et al., *Planck 2015 results. XIII. Cosmological parameters*, *A&A* **594** (Sept., 2016) A13, [1502.01589].

[5] C. Heymans, E. Grocutt, A. Heavens, M. Kilbinger, T. D. Kitching, F. Simpson et al., *CFHTLenS tomographic weak lensing cosmological parameter constraints: Mitigating the impact of intrinsic galaxy alignments*, *MNRAS* **432** (July, 2013) 2433–2453, [1303.1808].

[6] C. Heymans, L. Van Waerbeke, L. Miller, T. Erben, H. Hildebrandt, H. Hoekstra et al., *CFHTLenS: the Canada-France-Hawaii Telescope Lensing Survey*, *MNRAS* **427** (Nov., 2012) 146–166, [1210.0032].

[7] S. Joudaki, C. Blake, C. Heymans, A. Choi, J. Harnois-Deraps, H. Hildebrandt et al., *CFHTLenS revisited: assessing concordance with Planck including astrophysical systematics*, *MNRAS* **465** (Feb., 2017) 2033–2052, [1601.05786].

[8] H. Hildebrandt, M. Viola, C. Heymans, S. Joudaki, K. Kuijken, C. Blake et al., *KiDS-450: cosmological parameter constraints from tomographic weak gravitational lensing*, *MNRAS* **465** (Feb., 2017) 1454–1498, [1606.05338].

[9] T. Abbott, F. B. Abdalla, S. Allam, A. Amara, J. Annis, R. Armstrong et al., *Cosmology from cosmic shear with Dark Energy Survey Science Verification data*, *Physical Review D* **94** (July, 2016) 022001, [1507.05552].

[10] S. Joudaki, A. Mead, C. Blake, A. Choi, J. de Jong, T. Erben et al., *KiDS-450: Testing extensions to the standard cosmological model*, *ArXiv e-prints* (Oct., 2016) , [1610.04606].

[11] D. N. Limber, *The Analysis of Counts of the Extragalactic Nebulae in Terms of a Fluctuating Density Field.*, *ApJ* **117** (Jan., 1953) 134.

[12] M. Loverde and N. Afshordi, *Extended Limber approximation*, *Physical Review D* **78** (Dec., 2008) 123506, [0809.5112].

[13] P. Simon, *How accurate is Limber's equation?*, *A&A* **473** (Oct., 2007) 711–714, [astro-ph/0609165].

[14] T. D. Kitching and A. F. Heavens, *Unequal-Time Correlators for Cosmology*, *ArXiv e-prints* (Dec., 2016) , [1612.00770].

[15] J. N. Goldberg, A. J. Macfarlane, E. T. Newman, F. Rohrlich and E. C. G. Sudarshan, *Spin-s Spherical Harmonics and* ð, *Journal of Mathematical Physics* **8** (Nov., 1967) 2155–2161.

[16] D. A. Varshalovich, A. N. Moskalev and V. K. Khersonskii, *Quantum Theory of Angular Momentum*. World Scientific Publishing Co, 1988, 10.1142/0270.

[17] W. Hu, *Power Spectrum Tomography with Weak Lensing*, *ApJ* **522** (Sept., 1999) L21–L24, [astro-ph/9904153].

[18] A. Lewis and S. Bridle, *Cosmological parameters from CMB and other data: A Monte Carlo approach*, *Physical Review D* **66** (Nov., 2002) 103511, [astro-ph/0205436].

[19] A. Lewis, *Efficient sampling of fast and slow cosmological parameters*, *Physical Review D* **87** (May, 2013) 103529, [1304.4473].

[20] G. Chon, A. Challinor, S. Prunet, E. Hivon and I. Szapudi, *Fast estimation of polarization power spectra using correlation functions*, *MNRAS* **350** (May, 2004) 914–926, [astro-ph/0303414].

[21] K.-W. Ng and G.-C. Liu, *Correlation Functions of CMB Anisotropy and Polarization*, *International Journal of Modern Physics D* **8** (1999) 61–83, [astro-ph/9710012].